Thomson scattering on non-thermal atmospheric pressure plasma jets

Thomson scattering on non-thermal atmospheric pressure plasma jets

2015 Plasma Sources Sci. Technol. 24 054005

(http://iopscience.iop.org/0963-0252/24/5/054005)

IOP Publishing Plasma Sources Science and Technology

Plasma Sources Sci. Technol. **24** (2015) 054005 (15pp) doi:10.1088/0963-0252/24/5/054005

Thomson scattering on non-thermal atmospheric pressure plasma jets

Simon Hübner[1,6], Joao Santos Sousa[2], Joost van der Mullen[3,4] and William G Graham[5]

[1] Eindhoven University of Technology, 5600 MB Eindhoven, the Netherlands
[2] LPGP, CNRS & Univ. Paris-Sud, 91405 Orsay, France
[3] Université Libre de Bruxelles (ULB) 50 av. F.D. Roosevelt, 1050 Brussels, Belgium
[4] Fontys University of Applied Sciences, PO Box 90900 Tilburg, the Netherlands
[5] Centre for Plasma Physics, School of Mathematics and Physics, Queen's University Belfast, Belfast BT7 1NN, UK

E-mail: simon.huebner.physik@gmail.com, joao.santos-sousa@u-psud.fr, jvdmulle@ulb.ac.be and b.graham@qub.ac.uk

Received 27 April 2015, revised 29 July 2015
Accepted for publication 4 August 2015
Published 27 August 2015

Abstract

To characterize non-thermal atmospheric pressure plasmas experimentally, a large variety of methods and techniques is available, each having its own specific possibilities and limitations. A rewarding method to investigate these plasma sources is laser Thomson scattering. However, that is challenging. Non-thermal atmospheric pressure plasmas (gas temperatures close to room temperature and electron temperatures of a few eV) have usually small dimensions (below 1 mm) and a low degree of ionization (below 10^{-4}). Here an overview is presented of how Thomson scattering can be applied to such plasmas and used to measure directly spatially and temporally resolved the electron density and energy distribution. A general description of the scattering of photons and the guidelines for an experimental setup of this active diagnostic are provided. Special attention is given to the design concepts required to achieve the maximum signal photon flux with a minimum of unwanted signals. Recent results from the literature are also presented and discussed.

Keywords: Thomson scattering, laser diagnostic, atmospheric pressure plasma, low temperature plasma

(Some figures may appear in colour only in the online journal)

1. Introduction

The scattering of photons on material particles is a vast topic. On unbound electrons it is called Thomson scattering, a mechanism that can be seen as the non-relativistic limit of Compton scattering. The elastic scattering on bound electrons is known as Rayleigh scattering and the inelastic scattering of photons on molecules as Raman scattering. Mie scattering occurs on larger particles of the dimensions of the photon's wavelength. To study ionized gases, Thomson scattering (TS) is by definition ideal for experimental plasma characterization, as it delivers direct information about the density and energy distribution of free electrons. Due to the low scattering probability, TS was not observed experimentally until the late 1950s, when an anomalous reflection of radio waves in the earth's ionosphere was explained by this mechanism (Forsyth *et al* 1953). The major impact for laboratory applications came with the development of the first high power ruby lasers that allowed the use of TS on Tokomak plasmas (Peacock *et al* 1969). A ruby laser can deliver single pulses with energies of tens of joules. Such a laser, operated in burst mode, is well suited for the study of fusion-related plasmas, even in real time (van der Meiden *et al* 2006). However, for smaller and more reproducible laboratory plasmas, accumulation of many scattering events by a laser with high average output is preferable. The

[6] Author to whom any correspondence should be addressed.
Present address: Reactive Plasmas & EP2, Ruhr-Universität Bochum, 44780 Bochum, Germany.

advent of high peak power Nd:YAG type lasers with faster pulse repetition rates led to the breakthrough in the use of TS on non-thermal laboratory plasmas, where non-thermal refers to a much lower gas than electron temperature (Huang *et al* 1992, de Regt *et al* 1995, Kempkens and Uhlenbusch 2000, Muraoka *et al* 1998).

During the laser-plasma interaction, the electrons oscillate in the electric field of the laser beam. Due to these oscillations, the accelerated electrons will emit dipole electromagnetic radiation, which will be around the wavelength of the incident laser. If the electron density is sufficiently low so that an electron's oscillation is unaffected by neighbouring electrons this is described as incoherent Thomson scattering (Salpeter 1960). This will be the case for the non-thermal atmospheric plasmas discussed here since, for the typical electron temperature of 1 eV, coherent Thomson scattering only becomes significant for values of electron densities of about $n_e > 3 \times 10^{21}$. The signal processing from incoherent scattering is substantially simpler as the observed scattered spectrum is then a sum of individual scattering events (Evans and Katzenstein 1969).

High spatial resolution is achieved since only photons generated in the small intersection volume of the optical axis and the laser beam are detected. This volume can have diameters of less than 100 μm (Kono and Iwamoto 2004). The temporal resolution is determined by the laser pulse length or the gating of the detection system, whatever is shorter; TS with temporal resolution of down to 0.3 ns is reported in literature (Kieft *et al* 2004). These capabilities of TS are unmatched by all other diagnostic techniques for free electron parameters in atmospheric pressure plasmas.

However, significant issues for the use of TS originate from the very small value of the Thomson scattering cross section and the dipole-like scattered wavefront. While this will be explained more in detail later, the problem is illustrated in figure 1 which shows an estimate of the fraction of photons per second generated by a typical Nd:YAG laser and a TS collection system (see (Carbone *et al* 2015)). It is clear that for low electron densities, even with very high grade optics and a high quantum efficiency camera, only a very small signal can be expected.

With reproducible plasmas, the integration time can be increased substantially. The detection limit is considerably lowered and it is then given by the signal to noise ratio of the Thomson scattering signal with respect to the noise of the stray light, Rayleigh and Raman scattering. So, for example, TS in a few Pascal gas pressure plasma-reactors of about 0.5 m diameter has been used successfully to probe low temperature argon plasmas with electron densities as low as a few 10^{16} m^{-3} and electron energies up to about 14 eV. (Hori *et al* 1998, Crintea *et al* 2009).

2. Thomson scattering theory and realization

2.a. Laser plasma interaction

The spectral power $P_\lambda(\Delta\Omega)$ of the scattered radiation collected in the solid angle element ($\Delta\Omega$) is given by

$$P_\lambda(\Delta\Omega) = P_i n L \frac{d\sigma}{d\Omega} \Delta\Omega \phi_\lambda(\lambda) \quad (1)$$

where P_i is the incident laser power, L the length over which the observed laser-medium interaction takes place, n the density of the scattering particles, $d\sigma/d\Omega$ the differential cross section, while $\phi_\lambda(\lambda)$ contains the spectral information, assuming that $\int \phi_\lambda(\lambda)\, d\lambda = 1$. In the case of incoherent TS, the spectral information arises from the Doppler shift induced by the free electron motion. The wavelength shift is related to the 2D velocity plane given by the laser beam and the collection optics. The projection of this velocity distribution onto the 1D line-of-sight gives $\phi_\lambda(\lambda)$. It can be derived from basic principles (Evans and Katzenstein 1969) that for a Maxwellian distribution of the electrons the observed 1D velocity distribution is equivalent to the actual 3D distribution.

Expression (1) can be used to obtain the electron density and temperature by inserting the corresponding differential cross sections for TS

$$\frac{d\sigma^{TS}}{d\Omega} = r_e^2 (1 - \sin^2\theta \cos^2\psi) \quad (2)$$

Here, the scattering angle θ is the angle between the incident and the scattered wave vector, ψ the angle between the plane of scattering and the polarization of the incident beam and $r_e = e^2/(4\pi\varepsilon_0 m_e c^2)$ the classical electron radius. It is obvious that the setup should be chosen such that the polarization is perpendicular to the detection at $\psi = 90°$. Then the scattering angle can be chosen freely. However, with a $\theta = 90°$ arrangement, the stray light is minimized and the spatial resolution is at its optimum, as the detection beam is not skewed. The spatial resolution may be further improved by magnifying the projection of the detection volume so that it fully occupies the entrance slit of the spectrometer. Then, (2) equals $d\sigma^{TS}/d\Omega = r_e^2 = 7.94 \times 10^{-30}\ m^2 sr^{-1}$.

Equation (1) for the scattered laser light is also valid for Raman (RmS) and Rayleigh (RyS) scattering provided the appropriate cross sections are inserted. The strength of the different scattering mechanisms is thus primarily determined by the differential cross section. For illustration different values of $d\sigma/d\Omega$ are given in table 1.

The elastic scattering on atoms and molecules (RyS) depends strongly on the gas species, more precisely on their polarizability and on the wavelength (Sneep and Ubachs 2005). For atmospheric plasma jets, the ionization degree is low with about $n_e/N = 10^{-4}$–10^{-7}, where N is the neutral gas density. That means that the Rayleigh signal exceeds the TS signal by 3–5 orders of magnitude (see table 1). The RyS can be removed taking advantage of the fact that its spectral width is much smaller than that of TS. This is due to fact that both RyS and (incoherent) TS are based on the Doppler effect. The atoms being much heavier than electrons have a much smaller thermal velocity range. The removal of RyS signal can be done by for example using multiple spectrometers as will be explained more in detail later. Other techniques employ notch filters such as volume Bragg gratings (Glebov *et al* 2012, Klarenaar *et al* 2015), interference filters (Wesseling and

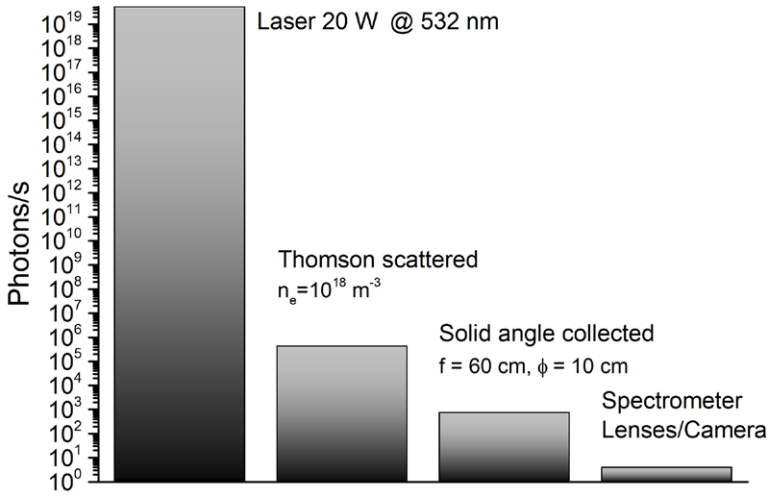

Figure 1. An impression of the extremely small fraction of collected photons; shown is the number of photons per second from a TS system (Carbone *et al* 2015) applied to a plasma with an electron density of $n_e = 10^{18}$ m^{-3}. The photons are collected within a laser-plasma interaction length of 1 mm in a solid angle determined by a lens with focal length $f = 60$ cm and a diameter of 10 cm. Eventually (after the spectrometer, lenses and camera) a fraction of less than 10^{-19} scattering events is registered.

Table 1. Overview of some differential scattering cross sections of different particles with 532 nm photons at scattering angles $\theta = 90°$ and $\psi = 90°$ from (2). (Molof *et al* 1974, Crosby *et al* 1977, Olney *et al* 1997, Sneep and Ubachs 2005, NIST database 2013). Note the large values for excited states.

Scattering type	Particle	Differential cross section [10^{-32} m^{2}sr^{-1}]
Thomson	e^-	794
Rayleigh	Ar	3.6
	Ar($^3P_2$)	3200
	He	0.056
	He($^1S_0$)	15 000
	N_2	3.9
	SF_6	21
Raman	N_2 (J–J' = 6–8)	0.054

Kronast 1996) or gas vapours (Bakker and Kroesen 2001, Lee and Lempert 2002). Another way to reduce the influence of Rayleigh scattering is to use an infrared laser, since RyS has a λ^{-4} dependence. This approach is however obstructed by the price of low sensitivity IR detectors (Bowden *et al* 1999) and the fact that working at invisible wavelengths requires care.

For the interference of TS with Raman scattering (RmS) the situation is more complicated. Again the RmS signal can be typically 1–3 orders of magnitude stronger than that of TS but the spectral shape of the RmS signal is much larger than that of RyS. RmS can have a similar spectral width as TS (see figure 2). Thus the RmS and TS signals can easily overlap in air containing plasmas and a careful identification of both signals is thus necessary (van Gessel *et al* 2012). The interference between TS and RmS strongly depends on the plasma conditions. High power densities will lead to high values of the electron density which in turn lead to high gas temperatures. This results in an enhanced dissociation of molecules which, combined with the high T_g and the Boltzmann distribution of the rotational states, leads to a very low RmS signal. The overlap of RmS with TS will thus be limited in plasmas of high power (density).

Laser induced fluorescence (LIF) can occur and might overlap largely within the spectral range of the TS signal. Either LIF is produced by surfaces in the vicinity of the laser or in optical components (Wesseling and Kronast 1996). That can be subtracted but its noise will reduce the detection limit. Another issue is LIF on plasma species. In He plasmas with a 532 nm laser LIF was observed (Wesseling and Kronast 1996, Hübner *et al* 2014), however the originating species is unknown; it could be $N_2^+(B^2\Sigma \rightarrow X^2\Sigma, v > 10)$ or a He excimer. In very strong LIF environments the choice of the laser wavelength might have to be reconsidered. In most cases the LIF decay is much slower than the immediate scattering events such as TS so that the signals can be temporally resolved recorded and disentangled (Soltwisch and Kaczor 1999).

2.b. Experimental realization

2.b.1. Laser delivery. In this section, the key issues of the implication of Thomson scattering measurements performed on non-thermal atmospheric pressure plasma jets are addressed through a description of a generic experimental setup. A basic assumption in our approach is that the plasma is *reproducible* so that the signal can be accumulated over many thousand laser shots. This requires that the plasma has no or little drift over a period of hours and implies that stochastic plasmas, such as moving filaments in a Dielectric Barrier Discharge are excluded. The ultimate goal of single shot TS on atmospheric pressure plasmas has so far only been realized in more dense systems such as an arc plasma at atmospheric pressure (Uchino *et al* 1982) or a microwave torch with n_e-values of about 10^{21} m^{-3} (van der Mullen *et al* 2007).

It is also necessary to be ensured that the laser itself does not perturb the plasma; for example too high laser power can heat the plasma by inverse Bremsstrahlung. It was found by

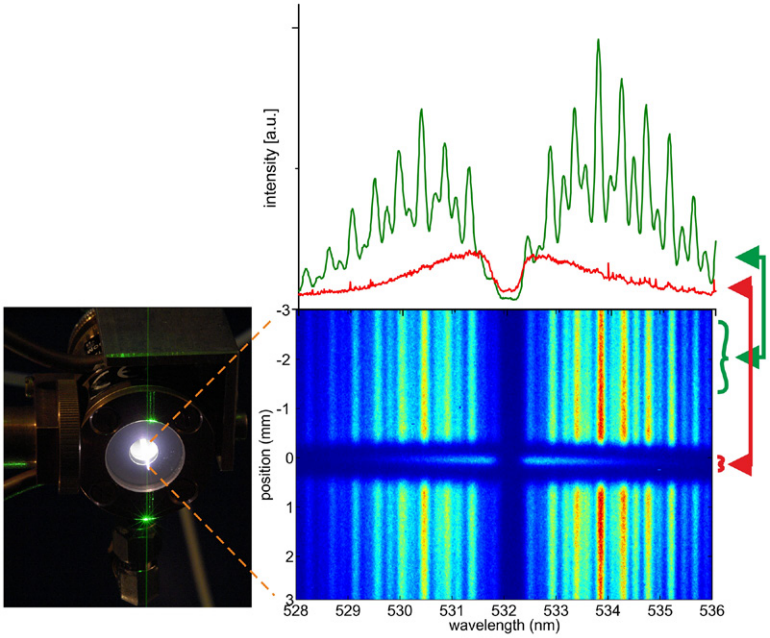

Figure 2. Laser scattering from an atmospheric microwave plasma (Surfatron) operated in argon at 50 W input power similar to (Palomares *et al* 2010, van Gessel *et al* 2012). The left image shows the laser beam intersecting the bright plasma flame. The bottom right figure shows the ICCD images created by scattered light after blocking the laser wavelength at 532 nm (suppression of RyS and stray light signal). The horizontal direction gives the wavelength distribution and the vertical depicts the spatial dimension along the laser-plasma intersection. Strong rotational Stokes and Anti-Stokes Raman scattering features are found due to the surrounding air. The smaller Thomson scattering signal is visible in the central argon flow. Upper right graph shows the intensity distribution of two cuts through the scattering signal that are used to calculate absolute values that are $n_e = 8 \times 10^{20}$ m^{-3} and $T_e = 1.2$ eV.

Carbone *et al* (2012) that taking into account electron-neutral and electron–ion inverse Bremsstrahlung leads to low theoretical values of the critical laser fluency (laser energy per area). Additionally, in a cold non-thermal plasma with an electron temperature of about 1.6 eV, with a laser beam spot of about 150 μm diameter and at a laser pulse energy of 100 mJ, they found by experiment that the electron temperature is increased by 10%. However, due to the high thermal conductivity, electrons can transfer heat to adjacent regions. Consequently in such a case of non-isolated electrons the increase of T_e is probably reduced significantly not only by heat conduction but also by ionization processes during the finite laser pulse length (de Vries *et al* 2005). Apart from laser-plasma heating one should realize that a laser can change the degree of ionization by photo detachment of negative ions or multi-photon dissociation, excitation or ionisation (Noguchi *et al* 2002, Muraoka and Kono 2011). All this can be readily checked by ensuring that there is a constant width and linear intensity response of the TS signal to the laser power.

Smaller pulse energies offered with a high repetition rate, can achieve high photon fluxes without such laser-plasma heating. One could think e.g. of a 100 kHz pulse rate Nd:YAG type laser systems producing pulses of 1 mJ.

However, working with high repetition rate laser systems implies that more plasma emission is collected. At the same time we should realize that plasma emission is normally not a big issue at non-thermal atmospheric pressure plasmas. That is in contrast to molecular low pressure plasmas or high power (close to thermal) plasmas, where in the first case molecular bands or in the second case continuum radiation readily dominates the TS signal (Muraoka and Kono 2011). Molecular radiation might be avoided by a tunable laser system.

The focusing of the laser beam into the plasma must ensure the best possible beam quality with a low beam divergence (low M^2 value). For that the use of apertures to block small angle scattered laser light is recommended. On the other hand the laser focusing is crucial to resolve the small atmospheric pressure plasmas. The focusing should be realized such that the *whole* radial extent of the laser beam is within the detection volume of the collection optics. This makes the signal independent of the beam diameter and small plasma displacements. The focusing has to be balanced against possible laser-plasma heating. The exiting laser beam should be effectively apertured and dumped to minimize scattered or reflected laser light. This is a major issue in micro-discharges (Kono and Iwamoto 2004) where there is inevitably a surface, for example an electrode, in the vicinity of the laser focus. The unwanted stray laser light can totally swamp the TS signal, as the latter has such a small scattering cross section. The stray light has more or less the same polarization as the laser, so it cannot be filtered effectively with polarizers. Here the choice of the scattering angle θ in relationship to surrounding solid surfaces can help. Where plasma electrodes form a very thin and narrow channel, a back-scattering confocal arrangement can be used with $\theta = 180°$ as was reported by Belostotskiy *et al* (2008). In that way, only one dimensional access is needed. This is at the price of higher stray light intensities. If the plasma is in a closed chamber for a controlled atmosphere, Brewster angled windows combined with apertures placed as far as possible from the detection volume help to reduce scattered light.

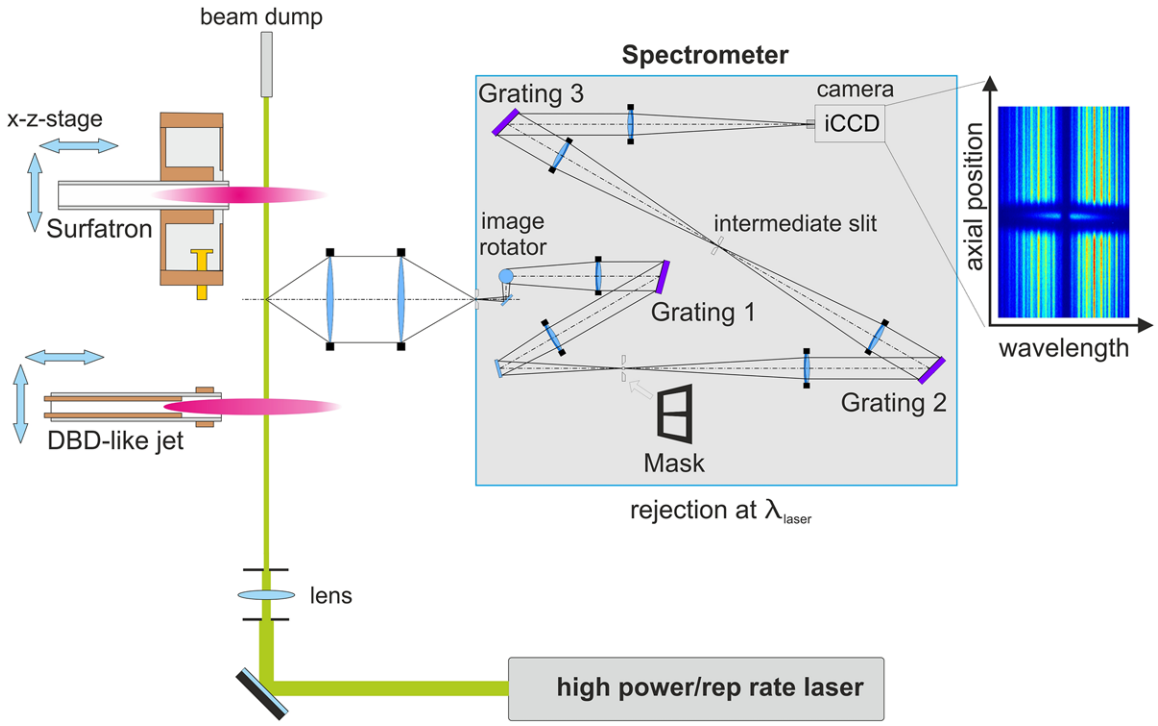

Figure 3. A sketch of a Thomson scattering set-up that can be applied to atmospheric pressure plasmas after van de Sande's thesis (2002). Two different plasma sources are depicted. These must be positioned so that the plasma- laser intersection takes place in the focal plane of the first light collecting lens. The large solid angle of that lens collects photons that are transferred to a spectrometer equipped with a high gain camera. This triple grating spectrograph is optimized for the rejection of photons within a narrow band around the laser wavelength which contains the large RyS and stray laser light components. Note that the dimensions in and outside the spectrometer are not to scale.

As previously mentioned (see figure 1), the collected solid angle is a critical issue for the signal strength. High grade imaging optics with small F-numbers is preferable. However, the limitation related to on-axis achromatic lenses is usually given by spherical aberration while off-axis mirrors are rather limited by astigmatism. Moreover, it should be kept in mind that the opening angle of the first optical element determines it for all further elements, since the etendue (light emitting surface times solid angle) is conserved. For a triple grating spectrometer this means that at least eight lenses and quite a large space are required.

2.b.2. Detection system. Here, the description of the detection system will focus on a triple grating spectrograph (TGS) (see figure 3). However, depending on the demands on filtering of the laser photons, other systems could be more suitable.

The collected photons are focused onto the entrance slit of the spectrograph. The slit is parallel to the axis of the laser beam, which allows spatially resolved images in the dimension along the laser beam. Inside the TGS, the beam has to be rotated, creating a vertical image of the slit. That is because it is highly preferable to remain at a constant beam height above the optical table while the vertical slit image is dispersed horizontally by the gratings. As previously mentioned, the polarization of the laser beam has to be perpendicular to the scattering plane. However, as the gratings in the spectrometer are usually polarization dependent, the beam polarization should be rotated after the scattering by a $\lambda/2$ plate.

A single spectrometer typically might have a stray light rejection of 10^{-3} (ratio of incident photons compared to the ones received at e.g. $\delta\lambda = 0.5$ nm). However, in the previous section it was shown that a RyS suppression of a factor of at least 10^{-5} is required. The use of a double spectrometer can provide that, as illustrated in figure 4. The first two identical gratings (G1 and G2) and the blocking mask form a notch filter for the central laser wavelength. Suppression of more than 6 orders of magnitude for signals that are $\delta\lambda = 0.5$ nm apart is readily achievable (van de Sande Thesis 2002). After the second grating, imperfections of the beam are removed by an intermediate slit that is similar to the entrance slit. The third grating resolves the actual spectral information. The gratings should have the appropriate spectral wavelength range and focal length. For the typical case of $T_e = 1$ eV that corresponds to a TS signal FWHM of $\lambda_{FWHM} = 2.5$ nm, a spectral range of about 10 nm is sufficient. That demands, with a typical 10–20 mm CCD detector, a dispersion of about $d = 2$ mm nm^{-1}. With that the width of the blocking mask w_{mask} can be calculated. The latter should be chosen to achieve the desired detection limit of the minimum electron energy. To record signals at $\delta\lambda = 0.5$ nm (0.1 eV) with a dispersion d and an entrance slit width of $w_{slit} = 250$ µm, the mask must not exceed $w_{mask} = 2 \times \delta\lambda d + w_{slit} = 2.25$ mm. However, the width of the mask might be chosen broader according to the stray light conditions as that will reduce unwanted light at the cost of low electron energy detection.

It is interesting to note that using an entrance slit of e.g. $w_{slit} = 250$ µm, to cover the whole laser beam, combined

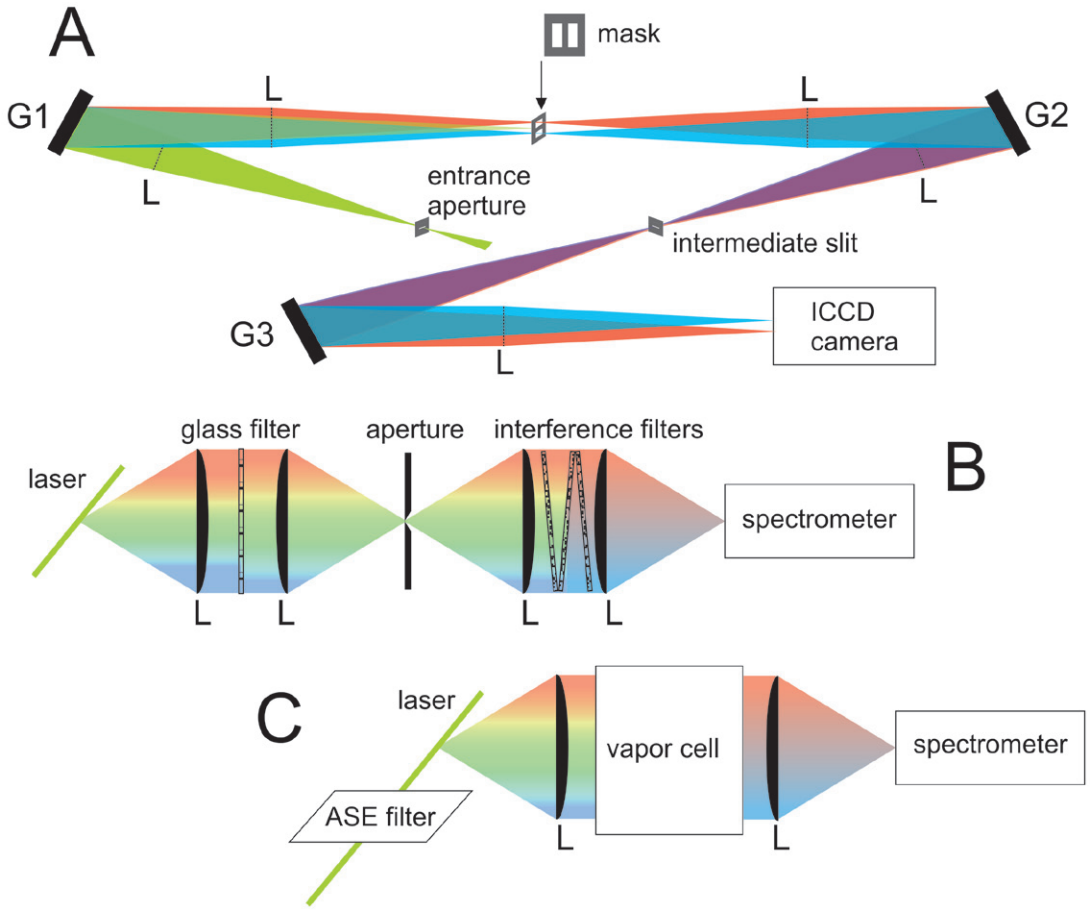

Figure 4. Simplified schemes for different laser light reduction techniques: (A) a triple grating arrangement with blocking mask; (B) a glass and interference filter set and (C) a vapor cell with a gas with a strongly absorbing transition which has a wavelength matched by a tunable laser. L denotes lenses and G gratings. The colors exaggerate the real wavelength spread.

with the requirement for the spectral bandwidth to be below $\lambda_{bw} = 0.3\,\text{nm}$, to be able to filter the laser wavelength and detect low energy electrons, requires a focal length of

$$f = \frac{w_{slit}\,\cos(\alpha)}{m\,g\,\lambda_{bw}} = 45\ \text{cm}$$

Here m is the order of diffraction, g the grating constant and α the angle of incidence on the grating. These values are taken from van de Sande (Thesis 2002).

Obviously the whole spectrometer must be placed in a completely black box and to avoid cross signals by e.g. higher/lower order diffraction, screens can be placed appropriately to absorb the light.

In order to identify unambiguously the RmS or plasma emission it is highly desirable to obtain a continuous spectrum by each laser shot. Therefore, the signal should be recorded by a multichannel detector (Kono and Nakatani 2000). The detector could be an array of photomultiplier tubes but today is now more likely to be a charge coupled detector with an intensifier (ICCD). The camera should be chosen for highest quantum efficiency, high gain and low dark noise and drift, while the frame rate is of less importance. The 2D camera image then resolves the TS spectrum both spatially, in the direction along the plasma-laser intersection, and in wavelength.

In practice, the focusing of the scattered laser light in the TGS is a crucial element in aligning the detection system. This can be realized by placing a low power diode laser with the same wavelength as the TS laser at the exact position of the camera (Carbone *et al* 2015). Then, the gratings and slits can be aligned without lenses. Next, the lenses are inserted one by one and focused correctly. Eventually, the laser beam should form a spot at the detection volume in the plasma.

Instead of a TGS, a single spectrometer could be used (Nedanovska *et al* 2011, Adress Thesis 2014). The setup of a single spectrometer with no dedicated laser wavelength filter is tempting as it is more straightforward. The laser scattering arrangement is very similar to that described in the sections above; the difference is that the measured laser scattering spectrum also contains the contributions from Rayleigh scattering. Consequently the drawback is the difficulty or sometimes inability to identify the possible small TS contribution in the environment of the huge Rayleigh and Raman scattering components.

As mentioned above, options other than spectrometers are possible to filter the laser wavelength (see figure 4). Interference filters were employed by Wesseling and Kronast (1996). A possible reduction of stray light by a factor of 10^{-6} is reported. However, a potential difficulty is the laser induced fluorescence in the filters. The use of gas vapor absorption

lines was also successfully used (Bakker and Kroesen 2001, Lee *et al* 2002). However, in order to shift the laser wavelength onto the absorbing transition, a high power dye or Ti:sapphire laser is needed from which the amplified spontaneous emission needs to be blocked. The option of using volume Bragg filters has so far only been realized for Raman spectrometers (Klarenaar *et al* 2015), but should be explored for Thomson scattering as well.

A general recommendation for the stray and Rayleigh scattered light suppression is difficult to give. In terms of low redistribution of light the TGS, or even more spectrometers, is unmatched. However, if compactness and easy handling is concerned the use of interference or Bragg filters might be more efficient. It is interesting to note that Raman scattering setups exhibit very similar issues concerning light suppression and top-notch systems employ also TGS or multiple filters.

2.c. Calibration of Thomson scattering

The rotational J–J' transitions of molecules lead to peaks in the Raman scattering spectrum, as can be seen in figure 2. This makes such a molecular spectrum ideal for the absolute calibration of both the intensity and the wavelength by using a multi-component fit (de Regt *et al* 1995).

The RmS calibration can be performed with any molecule that has a rotational constant that matches the detection wavelength range. The allowed transitions of $J' = J \pm 2$ lead to the red-shifted Stokes (+) and blue-shifted anti-Stokes (−) band with their characteristic intensity variation due to the Placzek–Teller coefficients. The total scattered power is

$$P^{\mathrm{RmS}}(\Delta\Omega) = P_{\mathrm{i}} L \Delta\Omega \sum_{J'=J\pm 2} n_J \frac{\mathrm{d}\sigma^{\mathrm{RmS}}_{J-J'}}{\mathrm{d}\Omega} \phi_\lambda(\lambda_{J-J'}) \qquad (3)$$

where $\phi_\lambda(\lambda_{J-J'})$ is also determined by the instrumental profile. The detection system does not need to resolve the individual rotational lines; an envelope fit is sufficient, However, if the signal intensity is expected to be high, better spectral resolution should be targeted. Nevertheless, because of the very little counts that TS provides, spectral signal binning is advised as the signal in each spectral wavelength interval must exceed the noise level.

In practice, the calibration is performed by using the ambient air or a vacuum vessel, with known gas pressure and temperature and *exactly* the same detection system. Consequently, the scattering signal is measured at a known gas density n_0 which can be related, together with the Boltzmann relation to obtain n_J. Using the respective cross sections, the wavelength integrated measured TS and RmS signals give the absolute electron density

$$n_{\mathrm{e}} = n_0 \frac{P^{\mathrm{TS}}\, \mathrm{d}\sigma^{\mathrm{RmS}}/\mathrm{d}\Omega}{P^{\mathrm{RmS}}\, \mathrm{d}\sigma^{\mathrm{TS}}/\mathrm{d}\Omega} \qquad (4)$$

With this calibration method, there is no need to determine the incident laser power, the plasma-laser interaction length or the solid angle $\Delta\Omega$ of the detection system. However, the absolute accuracy depends on the value of the respective Raman cross section. For example for N_2 an uncertainty of about 6% is expected based on the values for the polarizability given in the literature (Olney *et al* 1997). Using the Rayleigh signal (basically the $\Delta J = 0$ component) as a calibration is also possible, but then a careful measurement of the stray light contribution is needed. If so, this can be measured under vacuum conditions or in different gases with largely different RyS cross sections, with an extrapolation to a 'zero' cross section (Evans and Katzenstein 1969, Huang and Hieftje 1985).

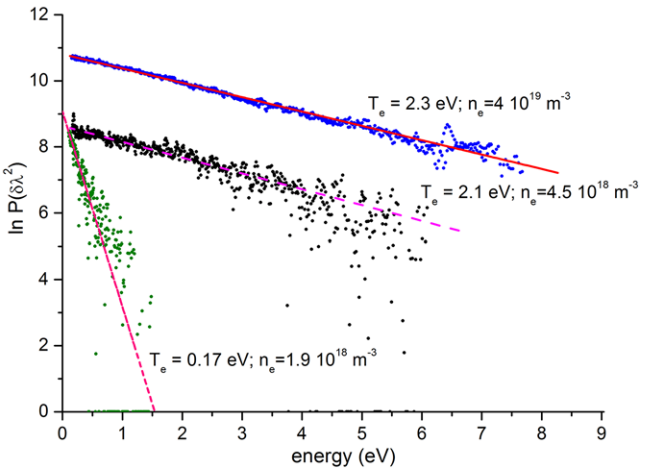

Figure 5. A logarithmic plot of the baseline corrected TS signal as function of $\delta\lambda^2$, giving part of the EEPF for a decaying plasma (Hübner *et al* 2013). Gaussian fits with the corresponding values are given. n_{e} values are derived by an absolute calibration. Note the inaccessibility of the EEPF for higher electron energies especially for low T_{e} values. Negative values are plotted as zero.

In case of the incoherent scattering, the spectral line width of Thomson scattered photons $\phi_\lambda(\lambda)$ is directly related to the Doppler shift induced by the electron velocity distribution function. A Maxwellian electron energy distribution function (EEDF) leads to a Gaussian distribution of the scattered photons. Inserting the corresponding function of $\phi_\lambda(\lambda)$ into (1) gives (van de Sande Thesis 2002)

$$P^{\mathrm{TS}}\, d\lambda = P_{\mathrm{i}} n L \frac{\mathrm{d}\sigma^{\mathrm{TS}}}{\mathrm{d}\Omega} \Delta\Omega \frac{1}{\Delta\lambda_{1/\mathrm{e}}\sqrt{\pi}} \exp\left[\left(-\frac{\delta\lambda}{\Delta\lambda_{1/\mathrm{e}}}\right)^2\right] \mathrm{d}\lambda \qquad (5)$$

with $\Delta\lambda_{1/\mathrm{e}}$ being the width of the spectral function at a fraction of 1/e of the maximum and $\delta\lambda = \lambda_{\mathrm{i}} - \lambda$. The electron temperature T_{e} can be derived via the Doppler formula to give

$$T_{\mathrm{e}} = \frac{m_{\mathrm{e}} c^2}{8\, k_{\mathrm{B}}\, \sin^2(\theta/2)} \left(\frac{\Delta\lambda_{1/\mathrm{e}}}{\lambda_{\mathrm{i}}}\right)^2 \qquad (6)$$

with λ_{i} the input laser wavelength. In practice, it is helpful to plot the logarithm of P_λ as a function of $(\delta\lambda)^2$, which gives a graph of the linearized electron energy distribution function (EEDF/$\sqrt{\mathrm{E}}$, known as the electron energy probability function, EEPF) (Huang *et al* 2000). With equation (6) the slope of the linear trend of this plot is equal to $-1/k_{\mathrm{B}}T_{\mathrm{e}}$ (see figure 5).

For the electron density, the spectral function $\phi_\lambda(\lambda)$ does not need to be known, only the total scattered signal as found from (4). That is because the number of scattered photons is directly proportional to n_{e}. As the signal can be very noisy, from equation (5) a fit of a Gaussian function of the data is

recommended with at least two fitting parameters, height and width. This yields the electron density, via the spectral area, and the temperature via equation (6).

As discussed in the work of Bowden *et al* (1999), the energy range over which the EEDF can be measured depends on the total electron density and the electron energy distribution in the context of the signal to noise ratio in the measured signals. In the case of their work for low pressure systems, the noise in the plasma emission or that of the TS signal itself determines the detection limit. However, as discussed above for plasmas in ambient air, also the noise of the Raman scattering plays a crucial role.

Effectively the method used in obtaining the data in figure 5 makes it possible to probe the mean energy and deviations from it, but does not provide information on the tail of the distribution function, simply because electrons with energies higher than a few $k_B T_e$ have much lower densities. This means that with TS in such plasmas it will be difficult to get insight into the effect of ionization processes on the EEDF and vice versa, at least not for plasmas with relatively low n_e and T_e values.

2.d. Comparison, advantages and disadvantages

There is a wide variety of experimental methods available to determine electron parameters in non-thermal atmospheric pressure plasmas. (Gigosos *et al* 2003, Ivkovic *et al* 2004, Chichina *et al* 2005, Balcon *et al* 2007, Ito *et al* 2010, Overzet *et al* 2010, Palomares *et al* 2010, Qian *et al* 2010, Hofmann *et al* 2011, Palomares *et al* 2012, Shashurin *et al* 2012, Sretenovic *et al* 2012, Bruggeman and Brandenburg 2013). However, the laser scattering techniques benefit from the straightforward interpretation of the raw data without much theoretical framework. A related example is RyS, where RyS gives direct values of the gas density N from which T_g can be obtained via the pressure. To validate this method, the rotational distribution of a molecular gas can be measured by optical emission or absorption spectroscopy or laser induced fluorescence. That only provides T_g if specific assumptions are satisfied, such as equilibrium distribution for the rotational states. This problem is addressed more extensively by Bruggeman *et al* (2014).

A technique that delivers information about the free electrons and that is easier to implement than TS is Stark broadening (Gigosos *et al* 2003, Ivkovic *et al* 2004, Palomares *et al* 2012). This spectroscopic technique relates the line broadening of an optical transition to the electric micro-field surrounding the emitter. *A priori* knowledge of the line shape as function of the electron density, temperature and perturber mass is necessary in order to use this method (Gigosos *et al* 2003).

As argued in Hübner *et al* (2014), the conditions for Stark broadening measurements in cold atmospheric pressure plasmas are not easy to satisfy. Especially in the case of a low gas temperature the Van der Waals broadening usually dominates over Stark broadening. For ambient conditions the hydrogen β-line has a pressure broadening of $\Delta\lambda_{VdW} \approx 100$ pm, while the Stark line width is about $\Delta\lambda_S \approx 2$ pm for $n_e = 10^{18}\,\mathrm{m}^{-3}$, and so it is even smaller than the corresponding fine structure. Moreover, this is a line-of-sight method and to measure local line broadenings out of the measured cumulative line shape, inverse Abel transformation has to be accomplished of many line shapes that are integrated over a non-uniform and unbounded plasma.

Because of the steep plasma gradients the demands for TS in terms of spatial resolution are as strict (resolution < 100 μm) as for Stark broadening. However, this is possible to tackle in TS as the laser focus defines the spatial resolution. Kono and Iwamoto (2004) achieved TS with a laser beam waist of about 25 μm to resolve small gradients while keeping the laser-plasma interaction low with a laser pulse energy of 4 mJ.

In Palomares *et al* (2010) it was found that the electron density measured in a microwave driven atmospheric plasma jet by passive methods such as H_β Stark broadening and continuum emission agreed to within the experimental uncertainties to those determined under the same conditions with TS. They also found that the use of absolute emission line intensities with a to determine T_e deviated from those determined by TS. This is of interest since line emission probes the tail of the electron energy distribution function, above the excitation potential of the emitting atoms, whereas TS probes the mean electron energy region (van de Sande *et al* 2002).

The electron density can also be obtained by current or impedance measurements or by using a simplified global model (Balcon *et al* 2007, Overzet *et al* 2010). However, these approaches usually rely on many uncertain values, such as the electron velocity, the plasma jet diameter, and the spatial distribution of the electron density and so provides only an estimate of the electron density.

Finally, electron densities can be also obtained from the change of the refractive index induced by the plasma. This can be measured by sending an electromagnetic wave (or laser) into the plasma. Scattering, absorption or phase shifting of microwaves is a well-known technique (Hutchinson 1990). However, as the dimensions of many atmospheric pressure plasmas are smaller than the wavelength of the electromagnetic waves typically used, either the scattering volume must be known precisely (Shneider and Miles 2005) or a shorter wavelength must be chosen. The former approach was successfully implemented by Sashurin *et al* (2015), while the latter was put into practice by Ito *et al* (2010) by using mm-wave heterodyne interferometry. Volume-integrated (in the first case) and line-integrated (in the second case) electron densities were obtained with good temporal resolution (down to ns). However, one should keep in mind that a variation in gas temperature or mixture might also change the refractive index and mask the effect of the electrons (Leibold *et al* 2000). Furthermore, the use of electromagnetic waves can only provide line- or volume-integrated electron densities.

Despite the obvious advantages of Thomson laser scattering, it should be kept in mind that the TS systems are not simple to be implemented and therefore unlikely to be applicable to systems in industrial environments (e.g. lack of access

Table 2. Selection of published TS experiments for various plasma sources at atmospheric pressure. Method describes the employed laser wavelength and SG, DG and TG denote single, double and triple spectrometer.

Plasma	Gas	n_e [10^{20} m^{-3}]	T_e [eV]	Method	Reference
20 kHz DBD-jet	He	0.005–0.15	0.1–1.6	532 nm + TG	Hübner *et al* 2014
5 kHz Needle-jet	Ar	0.01–0.7	0.1–3	532 nm + TG	Hübner *et al* 2013
RF 14.5 MHz, pulsed jet	Ar, Ar/air	0.05–0.2	0.2–2	532 nm + TG	Van Gessel *et al* 2013
DC microgap	Ar	0.3–0.9	0.7–1	526.5 nm + TG Backscattering	Belostotskiy *et al* 2008
MW 2.45 GHz jet	Ar	0.2–8	1.2–5	532 nm + TG	Van Gessel *et al* 2012
MW 2.45 GHz microgap	He/N2, Air	3–18	0.6–1.5	532 nm + TG	Kono *et al* 2004
RF 27 MHz ICP	Ar, Ar/H_2O	1–20	0.3–0.7	532 nm + SG	Huang *et al* 1992
MW 2.45 GHz torch	Ar	1–22	0.8–1.9	532 nm + TG	van der Mullen *et al* 2007
LIBS	He	100–800	1.4–1.6	532 nm + DG	Nedanovska *et al* 2011

to the plasma or the considerable investment in equipment). However in this context it can find value calibrating other less complicated techniques or plasma models.

3. Results of Thomson scattering measurements

For reviews on TS measurements of the electron properties in dense hot atmospheric pressure plasmas such as arcs (Uchino *et al* 1982, Snyder *et al* 1994), plasmas created by laser induced breakdown (Nedanovska *et al* 2011) or inductively coupled plasmas (de Regt *et al* 1995) the reader is directed to the reviews of Warner and Hieftje (2002) about spectro-chemical plasmas, or Muraoka and Kono (2011) on low temperature plasmas in general. This brief review will focus on published work in non-thermal atmospheric pressure plasmas. The material has been selected to illustrate facets of the use of TS in obtaining electron densities, temperatures and electron energy distribution functions. A summary is given in table 2.

Non-thermal plasma jets are generally created in an inert gas, often with up to a few percent added molecular species to generate reactive species for specific applications. The gas is generally flowed through a dielectric tube, often quartz or alumina with diameters from below 1 mm up to several mm. An electric field is applied within the vicinity of the tube using different driving circuits or electrode configurations. The frequency, pulse shape and magnitude of the applied voltages tend to define the features of the plasma. Irrespective of the driving pulse shapes and frequencies, gases or flow rates, the defining property of all the sources discussed here is, that there is a luminous plume, extending into the ambient air or controlled atmosphere from the exit of the primary plasma source. Most, but not all, reported TS measurements are made in this plume region. To date TS measurements have been reported in plasma jets driven by microwave, radio or kHz frequencies, sometimes in combination.

3.a. Microwave driven plasma jets

An example of a microwave driven plasma jet is the Surfatron as shown in figure 2, which is similar to one used in the measurements of van Gessel *et al* (2012). A 2.45 GHz MW cavity launches radiation along the jet axis, creating and sustaining

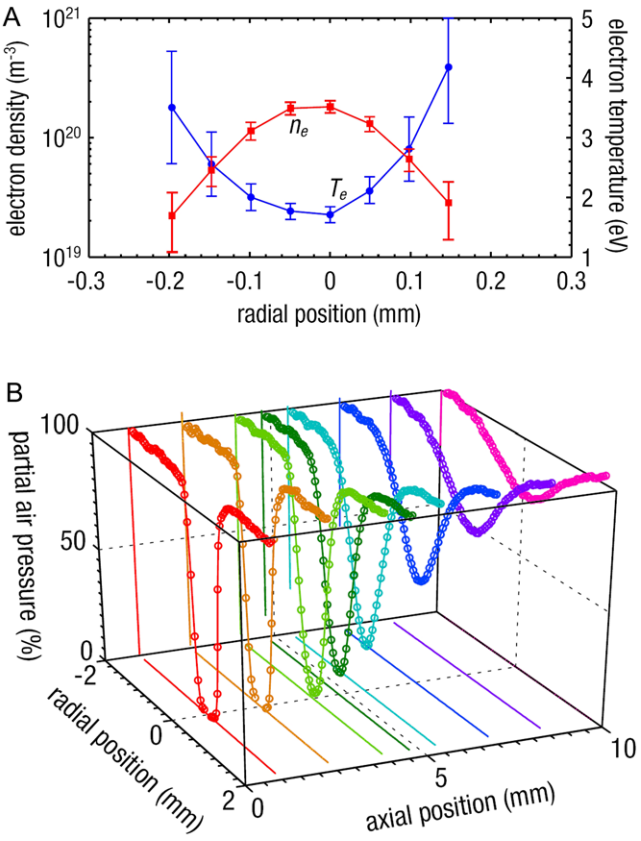

Figure 6. MW jet similar to that shown in figure 2. The jet was operated with a 1.0 slm flow of argon into ambient air. (A) The TS derived radial profile of the electron density and temperature measured at 5 mm downstream from the nozzle exit. (B) Measurement of the partial air pressure derived from the simultaneously measured Raman laser scattering. Reprinted with permission from van Gessel *et al* (2012) © 2012, IOP Publishing.

the plasma by generating a cylindrically symmetric surface wave (Moisan and Zakrzewski 1991) in a 0.8 mm diameter, air cooled quartz tube through which argon is flowing at 1 slm into the ambient air. The generator delivered a power of 50 W but the absorbed power in the plasma is unknown. Spatially resolved TS measurements were obtained for distances up to 10 mm from the end of the tube and with up to 10% air added to the argon gas flow.

Figure 6(A) shows some of the TS-derived results. It clearly shows the presence of a plasma with electron densities up to a

few 10^{20} m^{-3} and electron temperatures of a few eV. Figure 6 also illustrates the additional valuable information that can be obtained from TS measurements, since the Raman scattered signal from N_2 and O_2 is obtained simultaneously. This allows the determination of the spatial distribution of the air fraction as shown in figure 6(B) and the gas temperature (not shown). It clearly demonstrates that the plasma is confined to the argon gas stream. The Raman scattering also shows that the gas is heated up. Rayleigh scattering shows even that the plasma core gas temperatures reach up to 600 K. The lowest measurable electron density was of about 5×10^{18} m^{-3}, determined mainly by the plasma emission and unwanted scattered light (RmS).

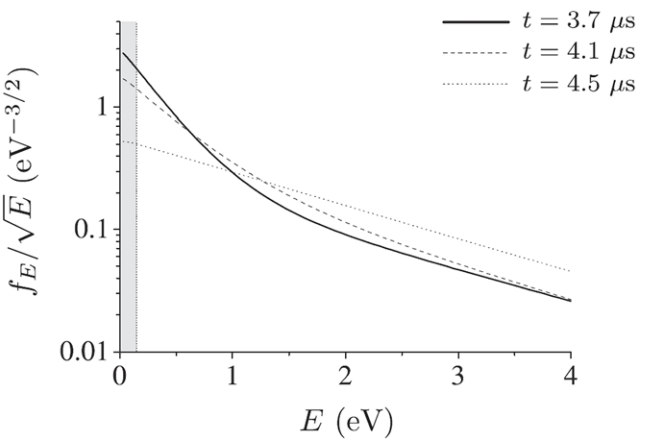

Figure 7. Non-Maxwellian EEPFs at different times during the decay phase of a 112 kHz driven plasma. For 3.7 and 4.1 μs, the EEPF is overpopulated above 1 eV with respect to a Maxwellian bulk T_e of 0.3 and 0.5 eV. Energies below 0.2 eV could not be measured. Reprint with permission from van de Sande *et al* (2002) © 2002, IOP Publishing.

3.b. Radio frequency driven plasma jets

Atmospheric pressure, radio frequency driven plasmas are either operated with an EM-field perpendicular to the gas flow, such as in a plate-plate or coaxial configuration, or an EM-field that is more or less parallel to the flow. In the latter case, the powered electrode is a cylindrical electrode or an internal, rod-type electrode (needle) in a dielectric tube. These jets can operate without a secondary grounded electrode, a cylindrical metal electrode on the outer surface of the dielectric cylinder or an electrode in the jet's effluent. Some of the first work on applying TS to a cold atmospheric plasma was reported by van de Sande *et al* (2002) in such a coupled system where the powered of two cylindrical electrodes on the outside of a 4 mm diameter quartz tube was driven with a rectangular shaped voltage at a frequency of 112 kHz at an average power of about 35 W. The second electrode was grounded. Helium was flowed through the tube at 0.35 slm. In this case the laser was passed axially through the discharge and the scattered light was observed through the quartz tube. So here the measurement was in the plasma source rather than in the jet. The measured electron density was found to be modulated with the driving frequency between 0.75 and 2.5×10^{19} m^{-3}. The electron temperature was modulated with values between 0.5 and 3.8 eV. However, the employed laser power of 400 mJ might have been sufficient to cause laser-plasma heating (see Carbone *et al* 2012)). Consequently, T_e is probably systematically overestimated. A feature of this work was that the electron temperatures were also determined using absolute spectral line intensity measurements giving values that deviated from the TS values. As discussed above, TS can also be used to determine the electron energy distribution. Here the TS spectra, as shown in figure 7 was found to deviate at some point in the RF cycle from a single Gaussian distribution, indicating that the electron energy distribution was not Maxwellian as assumed in the spectral line intensity analysis.

A time modulated RF frequency driven plasma jet was studied by van Gessel *et al* (2013). A pin electrode inside a 1.5 mm inner diameter glass tube was powered at 14.5 MHz which in turn was modulated with a 20 kHz square pulse with a 20% duty cycle. Two configurations of grounded electrode were used, one with a ring electrode around the tube and the other with a plate positioned 3 mm from the tube exit. Argon gas, with a few percent of admixed air, N_2 or O_2 was flowed through the tube at a rate of 1.0 slm. Figure 8 shows the TS results obtained at the end of the 20 kHz pulse. At least an order of magnitude higher electron density was found in the high electromagnetic field region between the electrodes, compared to what was found in the effluent region after the grounding plate.

3.c. High-voltage pulsed plasma jets

Plasma jets can also be generated in the geometries described above by applying high voltage sinusoids or pulses at 10's kHz frequencies to one of the electrodes. Time resolved imaging shows that the resultant ionization can occur as a guided streamer. Traveling ionization waves form a plasma channel with the plasma extinguished before the next voltage pulse or half cycle of alternating voltage (Lu *et al* 2012).

An example of TS measurements from a source operating with a 7 kV, 250 ns wide positive pulse at 20 kHz is shown in figure 9 based on Hübner *et al* (2014). In this case, the powered electrode is a hollow capillary inside a quartz tube enclosing the 4.5 slm He flow. The quartz has an inner diameter of 2.1 mm and outer diameter of 7.1 mm; around the tube at the height of the powered electrode is a grounded electrode placed. The plasma jet emerges out of the quartz tube at about 7 mm downstream from the powered electrode. A hollow plasma channel is formed that collapses downstream. Interestingly, the maximum electron density was found further downstream and not at the nozzle exit. Note that the densities in figure 9 were measured at different times, corresponding to the temporal maximum at each axial position. Mean electron energies of up to 2 eV were found (not shown) which decayed rapidly after the ionization wave has passed.

Adress (Adress Thesis 2014) studied the plasma plume of another dielectric barrier discharge-based, atmospheric pressure plasma jet, operating into ambient air with helium feed gas at 3 slm. An assembly of two sequential, cylindrical electrodes is used; the upstream is grounded while the downstream is powered. The tube has an inner diameter of 4 mm and the

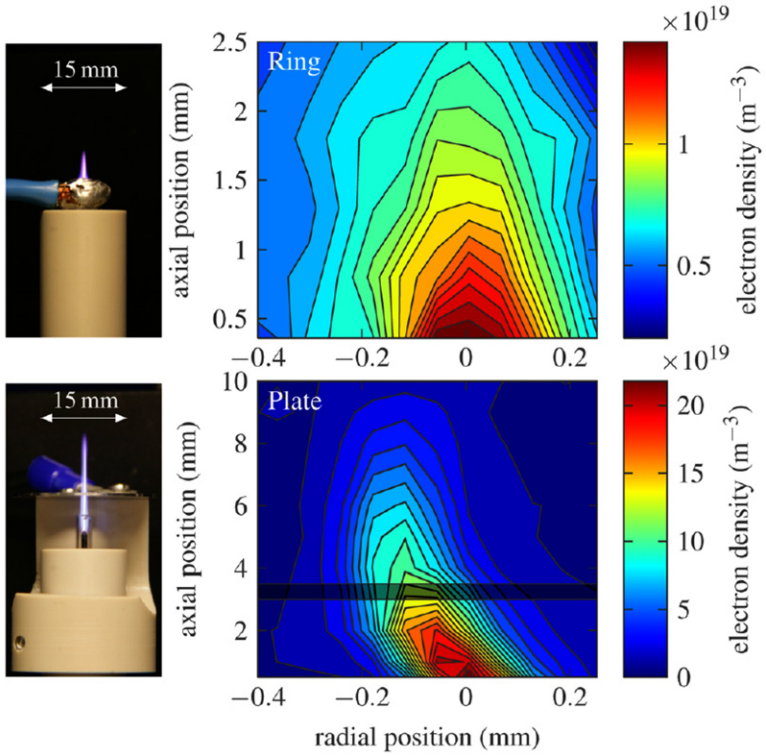

Figure 8. Images and spatially resolved electron density measurements from a modulated RF jet. Argon + 1% air gas was flowed at 1.0 slm into ambient air. Top figure with grounded, concentric electrode close to the tube exit. Bottom figure with a grounded plate 3 mm from the tube exit, indicated by a dark bar on the electron density map. The end of the quartz tube is at axial position zero. Reprinted with permission from van Gessel *et al* (2013) © 2013, AIP Publishing LLC.

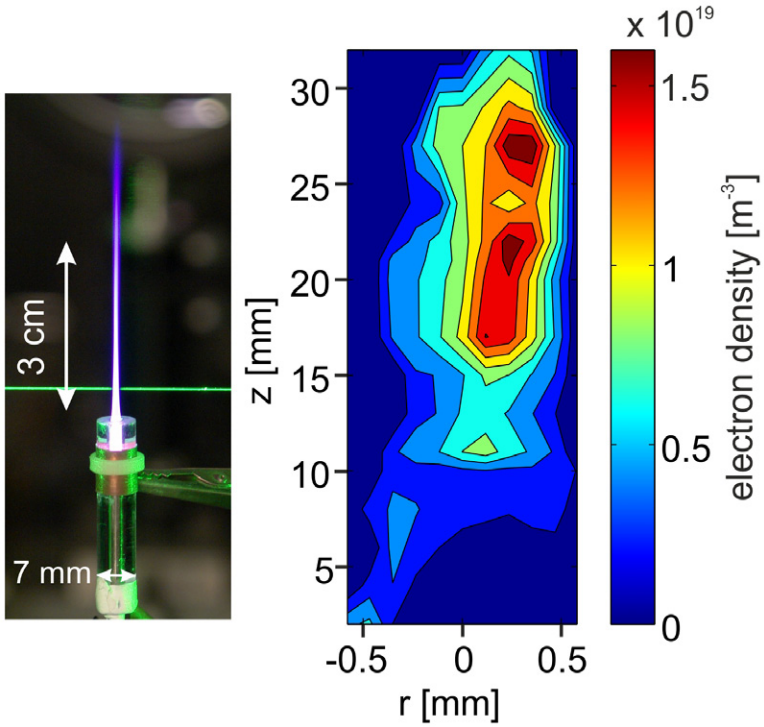

Figure 9. Pulsed DBD-like jet with a capillary inner high voltage electrode and a grounded outer ring, operated with a flow of He into ambient air, adapted from (Hübner *et al* 2014). For each z-position TS was recorded at the time of the maximum electron density (waveform shown in figure 10). The spatial distribution of the electron density shows its collapsing evolution. The $z = 0$ position corresponds to the end of the quartz tube.

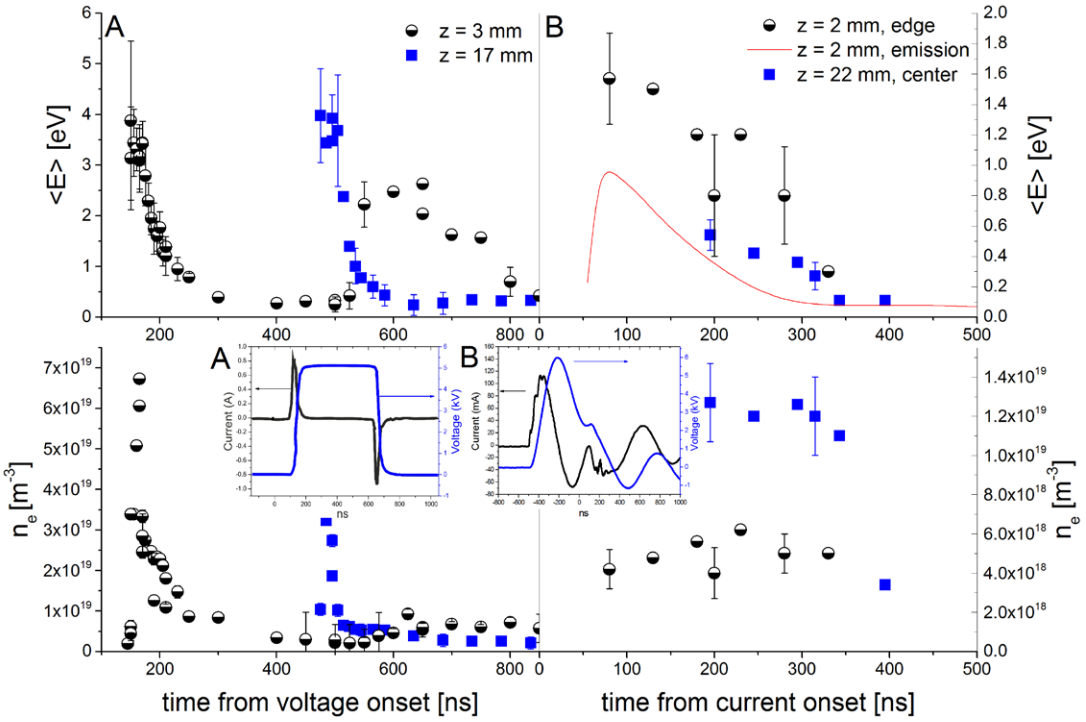

Figure 10. TS results from pulsed HV jets (A) Pin-type electrode HV jet with an Ar flow in ambient Ar, geometry is the same as in figure 6 without a grounding electrode. T_e and n_e show a very steep temporal decay. Re-ignition of the plasma at the end of the 500 ns voltage pulse is found close to the nozzle (Hübner *et al* 2013). (B) He DBD-like plasma jet in ambient air, same as in figure 9. T_e shows a monotonous temporal decay while n_e is almost constant (Hübner *et al* 2014). Note the respective voltage and current shape in the insets.

nozzle is also 4 mm downstream from the grounded electrode. The electrical waveform consists of a 6 kV positive pulse at 20 kHz with half width at half maximum of 2 μs.

Preliminary results indicate that electron densities at the centre of the plasma plume are about 5×10^{19} m^{-3} and the electron temperature 0.16 eV. These values increase radially to values of about 1.3×10^{20} m^{-3} and 0.25 eV at 2.2 mm from the centre. These results differ compared to (Hübner *et al* 2014), however, there are significant differences between the two experiments, for example, the electrode geometry and the voltage pulse shape.

Since TS provides temporal resolution in the nanosecond range, the ionization wave of the guided streamer can be probed directly. That gives unique insight into the excitation kinetics. In figure 10(A), the temporal evolution of a high voltage pulsed jet with an argon flow into ambient argon is shown (Hübner *et al* 2013). For different positions, the maximum value of the electron density and temperature of the guided streamer arrives at different times. In argon a steep decay of the energy and density of the electrons is found. However, different to that is the temporal decay of the He DBD-like jet in figure 10(B) (Hübner *et al* 2014). As in Ar the ionization front of the guided streamer arrives at different times, however a slower temporal decay and lower electron densities are found. The electrode configuration and applied voltage is not comparable, however, from the trends and other unpublished data it is concluded that the fundamental difference of the electron kinetics is due to the difference in feeding gas. Argon exhibits a more rapid decay than He, and indeed dissociative recombination rate coefficients are slightly faster for Ar, but as the densities are also much higher, electron-ion recombination reaction rates are faster. Another issue is the spatial distribution of the plasma, which is also different in both gases.

Shown is also the visible plasma emission which follows the electron temperature very closely. That can be understood if, in first approximation, the excitation balance consists only of electron impact excitation balanced by radiative decay, where the timescale of the latter is in the order of tens of ns.

Note that when exploring transient plasmas with TS, the jitter between laser and plasma pulse and the detection gate time set a temporal limit since multiple plasma pulses are averaged. Moreover, spatially varying filaments are always averaged.

3.d. Other micro discharges

Plasma sources which truly satisfy the word ‘micro’ are very challenging to access by TS. The small dimensions demand a well-defined small laser beam focus and high stray light suppression, as very strong signals from the surfaces in the laser vicinity will be produced.

Hassaballa *et al* (2012) performed TS on a modified plasma display panel cell. Two electrodes with a gap of 100 μm are embedded in glass coated with a protective MgO film. A dielectric-barrier discharge is then ignited with a 20 kHz, 240 V peak voltage on top of the dielectric at pressures of a few hundred mbar in Ne/Ar mixtures. Since the plasma is located very close to the surface, the laser beam path was prolonged and ‘cleaned’ with apertures. Electron densities were measured as

close as 60 μm from the surface. Another challenging setup is presented by Belostotskiy *et al* (2008) as mentioned before with a backscattering arrangement using a periscope in the laser beam path. An electrode gap of 600 μm powered by dc (50 mA, 310–350 V) in 300–700 mbar argon was studied. Due to the high power density electron densities as high as 4×10^{19} m^{-3} are reported.

Even smaller plasma dimensions are reported in the work Kono *et al* (2004). A micro gap was studied at atmospheric pressure consisting of two knife edges with 100 μm spacing in between. To insert the laser in that gap a very short focal length of 15 cm together with apertures along an extended laser beam path were used. That arrangement lead to a spatial resolution of 25 μm, however the issue of laser heating is likely to occur and therefore the laser power was reduced to 4 mJ per pulse. A microwave power of 100 W lead to peak electron densities of about 2×10^{21} m^{-3} in air, i.e. already slightly coherent TS with $\alpha \approx 0.3$.

All three given examples employ a TGS to filter the stray and RyS light. That underlines the conclusion of section 2.b in respect to the choice of the TGS for a high performance filtering system.

4. Summary

This paper focuses on an overview of the implementation of Thomson scattering to micro-scale atmospheric pressure plasma jets. This is a complex diagnostic and so details and issues requiring consideration for its proper use are discussed. Some typical measurements, from a variety of plasma jet systems, are also shown and discussed to illustrate its power in providing fundamental data on the properties of the electrons in plasma jets.

In summary the crucial issues in implementing Thomson scattering are

(a) Scatter and collect as much of the incident photon flux as possible. The laser power should be as high as possible, without perturbing the plasma, but also the solid angle of the collection optics must be optimized.
(b) Have a stable and reproducible plasma source. That is required as multiple laser shots are averaged and any drift or a stochastic nature of the plasma will alter the measured values.
(c) Ensure proper reduction of the stray light and unwanted scattering signals. This requires consideration of issues, such as the laser beam quality and the capability of spectral filters to suppress photons at adjacent wavelengths. The wavelength dependence of a spectrometer can easily make the wings of the laser spectra appear as a false TS Gaussian distribution.
(d) If the TS signal can be fitted to a Gaussian fit, the resultant electron temperature gives a mean electron energy value.

In conclusion TS is currently a powerful technique for probing the spatial and temporal behaviour and properties of the major, lower energy component of the electrons in a variety of non-thermal atmospheric pressure plasma jets. These measurements can be invaluable in validating and as input to simulations and models for such plasma jets. There are still major challenges in being able to fully explore a broader range of the electron energy distribution and to work in high pressure plasma systems with short scale or non-reproducible spatial and temporal structure.

Acknowledgments

One of the author (S H) thanks the 7FP Marie Curie ITN, RAPID for financial support.

References

Adress W 2014 Physics and application of an atmospheric pressure plasma jet *PhD thesis* Queen's University Belfast, UK
Bakker L P and Kroesen G M W 2001 Thomson scattering in a low-pressure neon mercury positive column *J. Appl. Phys.* **90** 3720
Balcon N, Aanesland A and Boswell R 2007 Pulsed RF discharges, glow and filamentary mode at atmospheric pressure in argon *Plasma Sources Sci. Technol.* **16** 217
Belostotskiy S G, Khandelwal R, Wang Q, Donnelly V M, Economou D J and Sadeghi N 2008 Measurement of electron temperature and density in an argon microdischarge by laser Thomson scattering *Appl. Phys. Lett.* **92** 221507
Bowden M D, Goto Y, Hori T, Uchino K, Muraoka K and Noguchi M 1999 Detection limit of laser thomson scattering for low density discharge plasmas *Japan. J. Appl. Phys.* **38** 3723–30
Bowden M D, Kudo H, Uchino K, Muraoka K and Noguchi M 1999 A thomson scattering measurement system based on an infrared laser *Japan. J. Appl. Phys.* **38** 4924–5
Bruggeman P and Brandenburg R 2013 Atmospheric pressure discharge filaments and microplasmas: physics, chemistry and diagnostics *J. Phys. D: Appl. Phys.* **46** 464001
Bruggeman P J, Sadeghi N, Schram D C and Linss V 2014 Gas temperature determination from rotational lines in non-equilibrium plasmas: a review *Plasma Sources Sci. Technol.* **23** 023001
Carbone E and Nijdam S 2015 Thomson scattering on non-equilibrium low density plasmas: principles, practice and challenges *Plasma Phys. Control. Fusion* **57** 014026
Carbone E A D, Palomares J M, Hübner S, Iordanova E and van der Mullen J J A M 2012 Revision of the criterion to avoid electron heating during laser aided plasma diagnostics (LAPD) *J. Instrum.* **7** C01016
Chichina M, Hubicka Z, Churpita O and Tichy M 2005 Measurement of the parameters of atmospheric-pressure barrier-torch discharge *Plasma Process. Polym.* **2** 501–6
Crintea D L, Czarnetzki U, Iordanova S, Koleva I and Luggenhölscher D 2009 Plasma diagnostics by optical emission spectroscopy on argon and comparison with Thomson scattering *J. Phys. D: Appl. Phys.* **42** 045208
Crosby D A and Zorn J C 1977 Dipole polarizability of 2 and 2 metastable helium measured by the electric deflection time-of-flight method *Phys. Rev.* A **16** 2
de Regt J M, Engeln R A H, de Groote F P J, van der Mullen J A M and Schram D C 1995 Thomson scattering experiments on a 100 MHz inductively coupled plasma calibrated by Raman scattering *Rev. Sci. Instrum.* **66** 3228
de Vries N, Zhu X, Kieft E R and van der Mullen J 2005 Time resolved Thomson scattering measurements on a high pressure mercury lamp *J. Phys. D: Appl. Phys.* **38** 2778–89

Evans D E and Katzenstein J 1969 Laser light scattering in laboratory plasmas *Rep. Prog. Phys.* **32** 207–71

Forsyth P A, Currie B W and Vawter F E 1953 Scattering of 56-Mc/s radio waves from the lower ionosphere *Nature* **171** 352

Gigosos M A, Gonzalez M A and Cardenoso V 2003 Computer simulated Balmer-alpha, -beta and -gamma Stark line profiles for non-equilibrium plasma diagnostics *Spectrochimica Acta* **58** 1489–504

Glebov A L, Mokhun O, Rapaport A, Vergnole S, Smirnov V and Glebov L B 2012 Volume Bragg gratings as ultra-narrow and multiband optical filters *Proc. SPIE 8428, Micro-Optics 2012, 84280C (June 1, 2012)*

Hassaballa B, Yakushiji M, Kim Y K, Tomita K, Uchino K and Muraoka K 2004 Two-dimensional Structure PDP micro-discharge plasmas obtained using Thomson Scattering *IEEE Trans. Plasma Sci.* **32** 127

Hofmann S, van Gessel A F H, Verreycken T and Bruggeman P 2011 Power dissipation, gas temperatures and electron densities of cold atmospheric pressure helium and argon RF plasma jets *Plasma Sources Sci. Technol.* **20** 065010

Hori T, Kogano M, Bowden M D, Uchino K and Muraoka K 1998 A study of electron energy distributions in an inductively coupled plasma by laser Thomson scattering *J. Appl. Phys.* **83** 1909

Huang M, Hanselman D S, Yang P and Hieftje G M 1992 Isocontour maps of electron temperature, electron number density and gas kinetic temperature in the Ar inductively coupled plasma obtained by laser-light Thomson and Rayleigh scattering *Spectrochim. Acta* B **47** 765–85

Huang M and Hieftje G M 1985 Thomson scattering from an ICP *Spectrochim. Acta* B **40** 1387–400

Huang M, Warner K, Lehn S and Hieftje G M 2000 A simple approach to deriving an electron energy distribution from an incoherent Thomson scattering spectrum *Spectrochim. Acta* B **55** 1397–410

Hübner S, Hofmann S, van Veldhuizen E M and Bruggeman P J 2013 Electron densities and energies of a guided argon streamer in argon and air environments *Plasma Sources Sci. Technol.* **22** 065011

Hübner S, Santos Sousa J, Puech V, Kroesen G M W and Sadeghi N 2014 Electron properties in an atmospheric helium plasma jet determined by Thomson scattering *J. Phys. D: Appl. Phys.* **47** 432001

Hutchinson I H 1990 *Principles of Plasma Diagnostics* (Cambridge: Cambridge University Press) pp 95–115

Ito Y, Sakai O and Tachibana K 2010 Measurement of electron density in a microdischarge-integrated device operated in nitrogen at atmospheric pressure using a millimetre-wave transmission method *Plasma Sources Sci. Technol.* **19** 025006

Ivković M, Jovićević S and Konjević N 2004 Low electron density diagnostics: development of optical emission spectroscopic techniques and some applications to microwave induced plasmas *Spectrochim. Acta* B **59** 591–605

Kempkens H and Uhlenbusch J 2000 Scattering diagnostics of low-temperature plasmas (Rayleigh scattering, Thomson scattering, CARS) *Plasma Sources Sci. Technol.* **9** 492–506

Kieft E R, van der Mullen J J A M, Kroesen G M W, Banine V and Koshelev K N 2004 Collective Thomson scattering experiments on a tin vapor discharge in the prepinch phase *Phys. Rev.* E **70** 056413

Klarenaar B L M, Brehmer F, Welzel S, van der Meiden H J, van de Sanden M C M and Engeln R 2015 Note: rotational raman scattering on CO_2 plasma using a volume Bragg grating as a notch filter *Rev. Sci. Instrum.* **86** 046106

Kono A and Iwamoto K 2004 High-spatial-resolution multichannel Thomson scattering measurements for atmospheric pressure microdischarge *Japan. J. Appl. Phys.* **43** 8A

Kono A and Nakatani K 2000 Efficient multichannel Thomson scattering measurement system for diagnostics of low-temperature plasmas *Rev. Sci. Instrum.* **71** 2716

Lee W and Lempert W R 2002 Spectrally filtered Raman/Thomson using a rubidium vapor filter *AIAA J.* **40** 2504–510

Leipold F, Stark R H, El-Habachi A and Schoenbach K H 2000 Electron density measurements in an atmospheric pressure air plasma by means of infrared heterodyne interferometry *J. Phys. D: Appl. Phys.* **33** 2268–73

Lu M, Laroussi M and Puech V 2012 On atmospheric-pressure non-equilibrium plasma jets and plasma bullets *Plasma Sources Sci. Technol.* **21** 034005

Moisan M and Zakrzewski Z 1991 Plasma sources based on the propagation of electromagnetic surface waves *J. Phys. D: Appl. Phys.* **24** 1025–48

Molof R, Schwartz H L, Miller T M and Bederson B 1974 Measurements of electric dipole polarizabilities of the alkali-metal atoms and the metastable noble-gas atoms *Phys. Rev.* A **10** 1131–140

Muraoka K and Kono A 2011 Laser thomson scattering for low-temperature plasmas *J. Phys. D: Appl. Phys.* **44** 043001

Muraoka K, Uchino K and Bowden M D 1998 Diagnostics of low-density glow discharge plasmas using Thomson scattering *Plasma Phys. Control. Fusion* **40** 1221–39

NIST Computational Chemistry Comparison and Benchmark Database, Release 16a 2013 August 2013, ed R D Johnson III (http://cccbdb.nist.gov/)

Noguchi M, Ariga K, Hirao T, Suanpoot P, Yamagata Y, Uchino K and Muraoka K 2002 Laser Thomson scattering measurements of negative ion density in a glow discharge plasma *Plasma Sources Sci. Technol.* **11** 57

Nedanovska E, Nersisyan G, Morgan T J, Hüwel L, Lewis C L S, Riley D and Graham W G 2011 Comparison of the electron density measurements using Thomson scattering and emission spectroscopy for laser induced breakdown in one atmosphere of helium *Appl. Phys. Lett.* **99** 261504

Olney T N, Cann N M, Cooper G and Brion C E 1997 Absolute scale determination for photoabsorption spectra and the calculation of molecular properties using dipole sum-rules *Chem. Phys.* **223** 59–98

Overzet L J, Jung D, Mandra M A, Goeckner M, Dufour T, Dussart R and Lefaucheux P 2010 RF impedance measurements of dc atmospheric micro-discharges *Eur. Phys. J.* D **60** 449–54

Palomares J M, Hübner S, Carbone E A D, de Vries N, van Veldhuizen E M, Sola A, Gamero A and van der Mullen J J A M 2012 H_β Stark broadening in cold plasmas with low electron densities calibrated with Thomson scattering *Spectrochim. Acta* B **73** 39–47

Palomares J M, Iordanova E, Gamero A, Sola A and van der Mullen J J A M 2010 Atmospheric microwave-induced plasmas in Ar/H_2 mixtures studied with a combination of passive and active spectroscopic methods *J. Phys. D: Appl. Phys.* **43** 395202

Peacock N J, Robinson D C, Forrest M J, Wilcock P D and Sannikov V V 1969 Measurement of the electron temperature by Thomson scattering in Tokamak T3 *Nature* **224** 488

Qian M, Ren C, Wang D, Zhang J and Wie G 2010 Stark broadening measurement of the electron density in an atmospheric pressure argon plasma jet with double-power electrodes *J. Appl. Phys.* **107** 063303

Salpeter E E 1960 Electron density fluctuations in a plasma *Phys. Rev.* **120** 1528–35

Shashurin A, Scott D, Zhuang T, Canady J, Beilis I I and Keidar M 2015 Electric discharge during electrosurgery *Sci. Rep.* **4** 9946

Shashurin A, Shneider M N and Keidar M 2012 Measurements of streamer head potential and conductivity of streamer column in cold nonequilibrium atmospheric plasmas *Plasma Sources Sci. Technol.* **21** 034006

Shneider M N and Miles R B 2005 Microwave diagnostics of small plasma objects *J. Appl. Phys.* **98** 033301

Soltwisch H and Kaczor M 1999 Potential and limitations of Thomson scattering in reactive plasmas *Proc. Front. Low Temp. Plasma Diag.* **3** 77

Sneep M and Ubachs W 2005 Direct measurement of the Rayleigh scattering cross section in various gases *J. Quant. Spectrosc. Radiat. Transfer* **92** 293–310

Snyder S C, Reynolds L D, Fincke J R, Lassahn G D, Grandy J D and Repetti T E 1994 Electron-temperature and electron-density profiles in an atmospheric-pressure argon plasma jet *Phys. Rev.* E **50** 519–25

Sretenovíc G B, Krstíc I B, Kovačevíc V V, Obradovíc B M and Kuraica M M 2012 Spectroscopic study of low-frequency helium DBD plasma jet *IEEE Trans. Plasma Sci.* **40** 2870–8

Uchino K, Muraoka T, Muraoka K and Akazaki M 1982 Studies of an impulse breakdown process in an atmospheric air using ruby-laser scattering diagnostics *Japan. J. Appl. Phys.* **21** L696

van Gessel B, Brandenburg R and Bruggeman P 2013 Electron properties and air mixing in radio frequency driven argon plasma jets at atmospheric pressure *Appl. Phys. Lett.* **103** 064103

van Gessel A F H, Carbone E A D, Bruggeman P J and van der Mullen J J A M 2012 Laser scattering on an atmospheric pressure plasma jet: disentangling Rayleigh, Raman and Thomson scattering *Plasma Sources Sci. Technol.* **21** 015003

van der Meiden H J *et al* 2006 10 kHz repetitive high-resolution TV Thomson scattering on TEXTOR: design and performance (invited) *Rev. Sci. Instrum.* **77** 10E512

van der Mullen J J A M, van de Sande M J, de Vries N, Broks B, Iordanova E, Gamero A, Torres J and Sola A 2007 Single-shot Thomson scattering on argon plasmas created by the Microwave Plasma Torch; evidence for a new plasma class *Spectrochim. Acta* B **62** 1135–46

van de Sande M 2002 Laser scattering on low temperature plasmas-high resolution and stray light rejection *PhD Thesis* Eindhoven University of Technology, The Netherlands

van de Sande M J, Deckers R H M, Lepkojus F, Buscher W and van der Mullen J J A M 2002 Time resolved electron density and temperature measurements on a capacitively coupled helium RF discharge *Plasma Sources Sci. Technol.* **11** 466–75

Warner K and Hieftje G M 2002 Thomson scattering from analytical plasmas *Spectrochim. Acta* B **57** 201–41

Wesseling H J and Kronast B 1996 Discrepancies between Thomson-light-scattering results and those obtained from E/N measurements in a helium glow discharge *Europhys. Lett.* **33** 273–8